

Surface Defect Healing in Annealing from Nanoporous Carbons to Nanoporous Graphenes

Kaoru Yamazaki,^{*b} Shunsuke Goto,^a Shunya Yoshino,^a Anna Gubarevich,^d Katsumi Yoshida,^d Hideki Kato^a and Masanori Yamamoto^{*ac}

Nanoporous graphene (NPG) materials have the pronounced electrochemical stability of the seamless graphene structures developed over the 3D space. We revisited the Raman spectra of nanoporous carbons (NPCs) synthesized using θ -/ γ -Al₂O₃ templates and NPGs converted from NPCs by annealing at 1800 °C to identify the type and density of defects. We found that both the NPCs and NPGs mostly consist of single-layered graphene with a few single vacancies and Stone–Wales defects. The density of vacancy defect *per* hexagon in the graphene sheet is estimated to be 10⁻² for NPCs, while the annealing reduced the value to 10⁻³–10⁻⁴ for NPGs. This supports the outstanding chemical and electrochemical stability of the novel porous carbon materials.

Introduction

Nanoporous graphene (NPG) materials^{1–6} enjoy the high electrochemical stability, high electrical conductivity, and flexibility of the continuous three-dimensional (3D) graphene architecture, with high surface area and nanoporosity. NPGs are synthesized by (i) chemical vapor deposition (CVD) of methane (CH₄) using nanoparticles of non-transition-metal oxides such as γ -alumina (γ -Al₂O₃)⁷ and MgO⁸ as the template, (ii) the subsequent acid etching for removing the metal oxides, and (iii) the annealing of the obtained nanoporous carbon (NPC) materials to give the 3D continuous architecture (Fig. 1). The mechanism of the initial NPCs formation at the early-stage CH₄-CVD reactions has been well-documented based on the reaction kinetics and quantum chemistry.^{1,3} The use of relatively inert CH₄⁹ as the gaseous carbon source is crucial for kinetically achieving the formation of mono-layered carbon.¹

We also revealed that the thermal treatment^{10–16} of NPCs at high temperatures under an inert atmosphere affords the corresponding NPGs by fusing the H-terminated edges,^{2,17} and this is the origin of the electrochemical stability of NPGs. This annealing following the CH₄-CVD synthesis will also improve the integrity of the graphene architecture by reducing the defect concentration, which is helpful to develop stable electrochemical devices using NPGs such as long-lived air–metal batteries *etc.*¹⁸ The quantitative evaluation of the defect type and concentration before/after annealing will be a starting point for the

development of state-of-the-art continuous porous carbon materials based on NPGs chemistry,^{1,2} but recent investigations on the structural changes upon annealing by changing the size of templates^{16,19} gave us a qualitative picture.

In this work, we carefully revisited the Raman spectra of NPCs and NPGs to quantitatively analyze the surface defects with aids of temperature-programmed desorption (TPD), X-ray diffraction (XRD), and nitrogen physisorption analysis. Raman spectroscopy has been used for the structure characterization of 2D graphenes and 1D carbon nanotubes,^{20–24} and it could also be applicable to the curved 3D analogues to provide insights into the structural disorders which breaks the translational symmetry, such as edges, defects, and grain boundaries of graphene-related materials.^{25–29} The TPD, based on the detection of desorbed molecules including H₂, CO, and CO₂, rationalizes the density of edges and adatoms,¹⁷ while the XRD and nitrogen physisorption validate the number of graphene layers in the carbon materials.²

We found that both the NPCs and NPGs mostly consist of single-layered graphene with a few single vacancies and Stone–Wales defects. In addition, a significant healing of the surface

^a Institute of Multidisciplinary Research for Advanced Materials Tohoku University, 2-1-1 Katahira, Aoba, Sendai 980-8577, Japan

^b RIKEN Center for Advanced Photonics, RIKEN, 2-1 Hirosawa, Wako, Saitama 351-0198, Japan

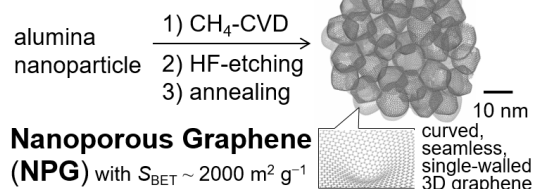
E-mail: kaoru.yamazaki@riken.jp

^c Department of Chemical Science and Engineering, Tokyo Institute of Technology Ookayama 2-12-1, Meguro, Tokyo 152-8550, Japan
E-mail: yamamoto@mol-chem.com

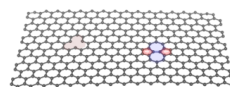
^d Institute of Innovative Research, Tokyo Institute of Technology 2-12-1 Ookayama, Meguro, Tokyo 152-8550, Japan

[†] Electronic Supplementary Information (ESI) available: synthetic details and characterisation of materials. See DOI: 10.1039/x0xx00000x

Previous Work



This Work



Structural Analysis by Raman Spectroscopy coupled with XRD, TPD, physisorption, and TEM

Fig. 1 Schematic of (top) the NPG synthesis by CH₄-CVD^{1,2} and (bottom) probing NPG structures by Raman spectroscopy.

defects in the 2D honeycomb lattice of sp^2 -carbons during thermal treatment of NPCs to NPGs at 1800 °C under inert atmosphere.

Experimental

Materials

Methane (CH_4) was purchased from Sumitomo Seika Chemicals Co., Ltd. with Pure grade (>99.0%) and SEG grade (>99.99%), and Taiyo Nippon Sanso Corp. with G1 grade (>99.999%). High purity γ -alumina nanoparticles (γ -ANPs, SBa-200; γ - Al_2O_3 , particle size: ~ 9 nm, specific surface area: $203 \text{ m}^2 \text{ g}^{-1}$) were donated from Sasol Limited. High purity θ -alumina nanoparticles (θ -ANPs, TM-100; θ - Al_2O_3 , particle size: ~ 10 nm, specific surface area: $120 \text{ m}^2 \text{ g}^{-1}$) were from Taimei Chemicals Co., Ltd. All chemicals were used as received unless otherwise noted.

Synthesis of Carbon Materials^{1,2,4}

Synthesis of NPC and NPG using θ -ANPs (TM-100) and γ -ANPs (TM-300) as the templates were reported previously,^{1,2,4} and the modified procedure was used to prepare the carbon materials for this work. γ -ANPs (SBa-200, Sasol Limited.) with a BET surface area of $200 \text{ m}^2 \text{ g}^{-1}$ was used as the nanosized template for the synthesis of single-walled 3D nanographene by chemical vapor deposition of CH_4 (CH_4 -CVD), ca. 2 g of SBa-200 was mixed with well-sieved quartz sand (ca. 7–8 g, Wako Pure Chemical Industries). The mixture was placed either in a horizontal or vertical quartz chamber, then heated to 1173 K (900 °C) at a rate of 10 – 15 K min^{-1} under a steady-flow of Ar (90 – 225 mL min^{-1}). The temperature was maintained for 10 – 30 min, and a mixture of CH_4 (20 – $31 \text{ vol}\%$) and Ar (80 – $69 \text{ vol}\%$) was then introduced to the chamber for 120 – 130 min at 1173 K for γ -alumina nanoparticles-catalyzed CH_4 -CVD. The temperature was maintained for 10 – 30 min under a steady flow of Ar. The chamber was then cooled down to room temperature, and the quartz sand was separated by sieving to obtain the carbon/alumina composite.

The weight ratio of the carbon deposition in the carbon/alumina composite was determined *via* thermogravimetry to calculate the average number of graphene layers as previously reported. The obtained carbon/alumina composite was immersed in an aqueous solution of HF (46 – $47 \text{ wt}\%$, 100 – 200 g , Wako Pure Chemical Industries) at room temperature for 5 h with agitation using a shaker (Reciprocal Shaker NA-201N, Nissin) to remove the template. Then, the aqueous solution was filtered using a hydrophilic PTFE membrane filter (Advantec H100A047A or H050A047A, Toyo Roshi Kaisha, Ltd., $\phi = 0.50$ or $1.00 \mu\text{m}$), and the residue was washed with an aqueous solution of HF (46 – $47 \text{ wt}\%$, 200 g , Wako Pure Chemical Industries) and water several times.

When more than 2 g of alumina was used, the template could not be fully removed. In this case, the chemical etching process with HF was repeated. The carbon on the filter was then washed with water 5 times. After the filtration, the wet sample was immersed in an organic solvent (acetone or isopropyl alcohol), and the mixture was stirred at 323 K (50 °C) for 6 h in total. Water was substituted with organic solvents to prevent the graphene architecture from shrinking under the intense capillary force of water. The solvents were then filtered off on a hydrophilic PTFE membrane, and the obtained carbon was dried

under vacuum at 373 K (100 °C) overnight to give the nanoporous carbon materials (NPCs). The average number of graphene walls n_{gra} was calculated to be ~ 1.1 by the TG analysis using an equation mentioned in the Table 1. NPCs were then annealed at 2073 K (1800 °C) in an induction heating furnace³⁰ or tabletop high temperature electric furnace for 0.5 – 1 h under a steady flow of Ar to afford the nanoporous graphene materials (NPGs).

Analysis of Obtained Materials

Wide-angle powder XRD patterns of the obtained samples were recorded using an X-ray diffractometer (Rigaku, MiniFlex 300/600) with Cu $K\alpha$ radiation ($\lambda = 1.5406 \text{ \AA}$) generated at 40 kV and 15 mA . Nitrogen physisorption measurements were conducted at 77 K using a volumetric sorption analyzer (BEL Japan, Belsorp). The specific surface area (S_{BET} in $\text{m}^2 \text{ g}^{-1}$) was calculated according to Brunauer–Emmett–Teller (BET) method in a pressure range of $P/P_0 = 0.05$ – 0.30 for the mesoporous materials,³¹ while $P/P_0 = 0.01$ – 0.05 was used for the microporous materials.³²

Raman spectra were obtained at room temperature by excitation at 532.2 nm with an Ar laser (100 mW) using a spectrometer (Jasco NRS-3300FL). The exposure time for the measurements was 120 s , and 10 scans were accumulated. The Raman shift was calibrated by the G band (1582 cm^{-1}) of the external standard, HOPG³³ or high quality graphite sheet (Toyo Tanso, PF-UHP). Nanoscale analysis of obtained carbon materials was conducted using a transmission electron microscope (Topcon EM-002B) at an accelerating voltage of 200 kV . The lattice resolution for the TEM measurements was 0.14 nm . The exposure time for the high-magnification TEM measurements was 1 – 10 s .

Results and Discussion

First, we measured the Raman spectra of NPCs and NPGs synthesized using θ -/ γ - Al_2O_3 as the templates (see the ESI[†] for the details of the method). The Raman spectra $I(E)$ of NPC and NPG synthesized using the θ - Al_2O_3 template were taken from our previous report.² We then deconvoluted these Raman spectra by the linear combination of normalized Voigt functions $V_i(E)$ ^{34–36} and the M -th order polynomial background $B_M(E) = \sum_{m=0}^M b_m E^m$ (b_m : constant) against the Raman shift E , as

$$I(E) = \sum_i A_i V_i(E; \epsilon_i, \Gamma_i, s) + B_M(E) \quad (1)$$

where A_i , ϵ_i , and Γ_i are the integrated intensity, peak position, and half width at half maximum (HWHM) of the Lorentzian function of peak i , respectively. s represents the full width at half maximum (FWHM) of the Gaussian function, which is the instrumental function. We set $M = 1$ for NPC and NPG synthesized with θ - Al_2O_3 , and zeolite-templated carbon³⁷ (ZTC), $M = 2$ for stacked NPC and NPG, $M = 3$ for NPG synthesized with γ - Al_2O_3 , and $M = 7$ for NPC synthesized with γ - Al_2O_3 to improve the numerical stability of the deconvolution procedure. We fixed s at 13.7 cm^{-1} , according to the energy resolution of the spectrometer. The other parameters are fully optimized using a least-squares fitting procedure. Each peak intensity $I_i(\epsilon_i)$ was evaluated as $I_i(\epsilon_i) = A_i V_i(\epsilon_i)$.

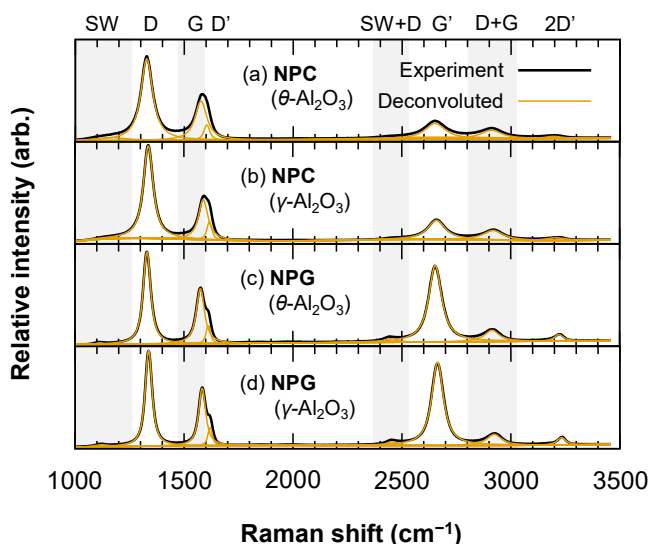


Fig. 2 Experimental (black) and deconvoluted Raman spectra (with the polynomial background, orange) of (a) NPC (θ -Al₂O₃), (b) NPC (γ -Al₂O₃), (c) NPG (θ -Al₂O₃), and (d) NPG (γ -Al₂O₃). Templates are specified in parenthesis. As previously reported,² all measurements were performed at 2.33 eV (532 nm).

The measured Raman spectra and deconvoluted peaks of NPCs synthesized using θ -Al₂O₃ (NPC (θ -Al₂O₃)) and γ -Al₂O₃ (NPC (γ -Al₂O₃)) are shown in Figs. 2a and 2b, respectively. Eight pronounced peaks are observed in each spectrum, some of which including D', D+G, and 2D' peaks have not been analyzed.² By the Raman spectra, XRD, and S_{BET} , we found that the NPCs and NPGs are mainly monolayer graphene with single vacancies³⁸ and heptagons/pentagons^{39,40} such as Stone–Wales (SW) defects.^{38,41–44}

We found that NPCs consists mainly of single-layer graphene. Here, we focus on the NPC synthesized with the θ -Al₂O₃ template (NPC (θ -Al₂O₃)) since the Raman spectra (Fig. 2b) and structural parameters were very close to those of NPC (γ -Al₂O₃) based on Raman spectra,

TPD, and XRD. For NPC (θ -Al₂O₃), the G band at 1577 cm⁻¹ in the Raman spectrum (Fig. 2a) and the in-plane 10 diffraction of turbostratic carbons in the XRD pattern (Fig. 3) indicate that NPC (θ -Al₂O₃) surely has a graphene structure. The single-layered graphene architecture of the NPC is supported by the downshifted G' band^{33,45} at 2651 cm⁻¹ as compared with that of the stacked analogue of graphite (~2700 cm⁻¹),³³ which is fitted by a single component.⁴⁶ The high gravimetric surface area ($S_{\text{BET}} = 2300 \text{ m}^2 \text{ g}^{-1}$, Fig. S1 and Table 1) approaches that of ideal single-layer graphene (2627 m² g⁻¹).

The weak and broad 002 diffraction peak in the XRD pattern also indicates that the single-layered structure is dominant for NPC. The probability distribution of the number of graphene layers ρ_ℓ is described by the Poisson distribution of mean number of layers \mathcal{L} as^{47–49}

$$\rho_\ell = \frac{(\mathcal{L} - 1)^{\ell-1}}{(\ell - 1)!} \exp[-(\mathcal{L} - 1)] \quad (2)$$

Here, $\ell - 1$ means the number of stacking and $\mathcal{L} - 1$ is its average. We plotted Eq. 2 for NPCs with setting $\mathcal{L} = n_{\text{gra}}$, obtained by the TGA in Table 1 and Fig. 3c. For NPC (θ -Al₂O₃) ($n_{\text{gra}} = 1.05$) as an example, 95% of the NPCs exit as the mono-layer graphene ($\ell = 1$) and the rest of 5% are the multilayer domains ($\ell \geq 2$). The minor multilayer domain contributes to the weak and broad 002 peak in its XRD pattern.

The existence of the D band at 1328 cm⁻¹, D' band^{26,51,52} at 1603 cm⁻¹, D+G band at 2909 cm⁻¹, and 2D' band at 3195 cm⁻¹ indicates that the NPC contains certain disorders.⁴⁶ The spectral parameters from the deconvolution of the Raman spectrum are summarized in Tables 1 and S1. The intensity ratio between the G' and G bands ($I_{\text{G}'}/I_{\text{G}}$) monotonically decreases with increasing disorder.⁵³ The $I_{\text{G}'}/I_{\text{G}}$ ratio of NPC (θ -Al₂O₃) is 0.43, which is smaller than that of pristine graphene ($I_{\text{G}'}/I_{\text{G}} \sim 3$).⁵³

The major disorders in NPCs are single vacancies and SW defects. The type of disorder can be qualitatively analyzed by the intensity ratio between the D and D' bands, $I_{\text{D}}/I_{\text{D}'}$.⁵¹ The $I_{\text{D}}/I_{\text{D}'}$ of NPC (θ -Al₂O₃) is 5.33. This indicates that these NPCs have both vacancies and grain boundaries since the $I_{\text{D}}/I_{\text{D}'}$ values lie between that of graphene dominantly with vacancies (~7) and grain boundaries (~3.5).⁵¹ The shoulder peak at 1163 cm⁻¹ proves the existence of SW defects.^{42,51,54} The small peak at 2454 cm⁻¹ can

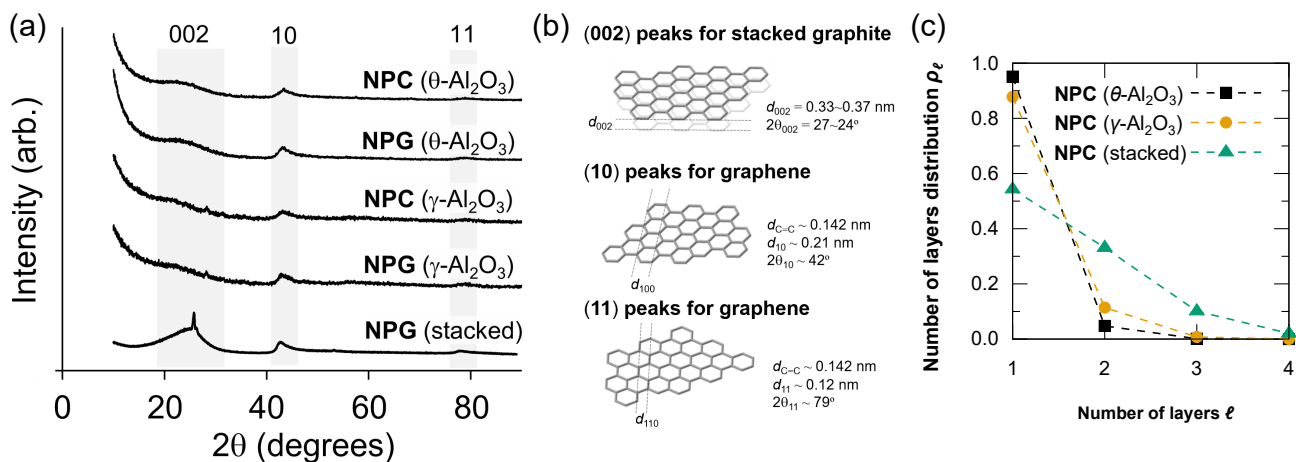


Fig. 3 (a) XRD patterns of NPCs, NPGs, and their stacked analogues either with θ -Al₂O₃ or γ -Al₂O₃ as the template. (b) Schematic of the origin of each diffraction. (c) Probability of discrete number of the stacked carbon layers calculated by Eq. 2 at a specified nominal layer of carbon deposition. $\mathcal{L} = n_{\text{gra}}$ were set to be 1.05 for NPC (θ -Al₂O₃), 1.13 for NPC (γ -Al₂O₃), and 1.61 for NPC (stacked) as shown in Table 1.

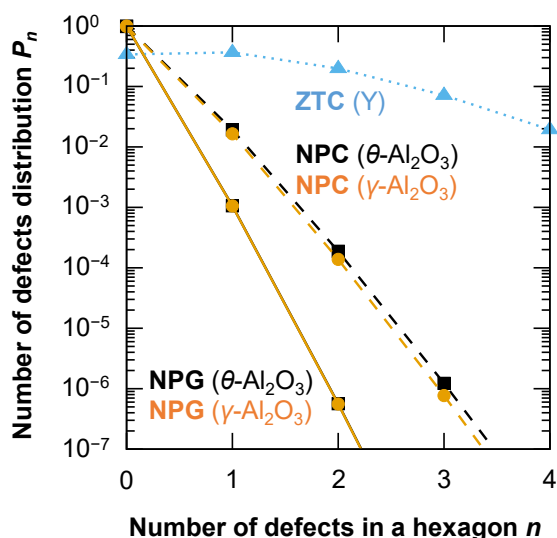


Fig. 4 Probability that a hexagonal ring has n defects, P_n , for **NPCs** (dashed line), **NPGs** (solid lines), and **ZTC** (blue dotted line) calculated from Eq. 2 with the values of λ_{Raman} displayed in Table 1. Templates are specified in parenthesis.

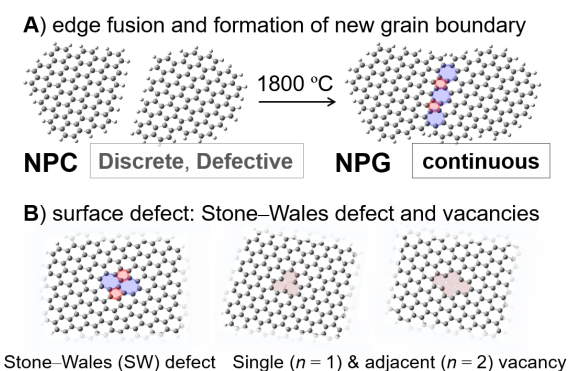


Fig. 5 (A) Edge fusion and formation of new grain boundary during the conversion from **NPC** to **NPG**² and (B) various surface defects, including grain boundary ($l_D/l_D \sim 3.5$) and vacancy defects ($l_D/l_D \sim 7$).⁵¹

be attributed to the SW+D band. The small amounts of gases evolved during the TPD analysis (N_{total} in Table 1) indicate the minor presence of edges (*vide infra*).

The mean distance between defects, R , is related to the intensity ratio of the D and G bands, $I_D/I_G(R)$, as²⁷

$$I_D/I_G(R) = C_A \frac{r_A^2 - r_S^2}{r_A^2 - 2r_S^2} \left[\exp\left(-\frac{\pi r_S^2}{R^2}\right) - \exp\left(-\frac{\pi(r_A^2 - r_S^2)}{R^2}\right) \right] + C_S \left[1 - \exp\left(-\frac{\pi r_S^2}{R^2}\right) \right] \quad (3)$$

where $r_S = 1.00$ nm is the mean radius of the structurally disordered region and $r_A = 3.00$ nm is the mean radius of the activated region where the graphitic structure is mostly conserved but the symmetry-breaking structure enhances the D band. $C_A = 4.2$ and $C_S = 0.87$ are parameters that describe the strength of the influences of the structurally disordered and activated regions on the intensity of the D band, respectively.²⁷ The I_D/I_G of **NPC** (θ - Al_2O_3) is 2.12 and the mean distance between the defects in **NPC** (R_{NPC}) can be estimated to be 1.64 nm by solving Eq. 3 for $I_D/I_G(R) = 2.12$.

The formation of multiple defects on a hexagonal ring is negligible in all **NPCs**, independent of the template, based on the Poisson distribution.^{55–57} The probability that a hexagonal ring has n defects (P_n) can be roughly estimated by a Poisson distribution:

$$P_n = \frac{\lambda^n}{n!} \exp(-\lambda) \quad (4)$$

where $\lambda \equiv 1/N_{\text{ring}}$ is the mean probability that a hexagonal ring has one defect (SW or vacancy). When considering **NPC** (θ - Al_2O_3) as an example, the single, double, and triple defect formation probabilities, P_1 , P_2 and P_3 , are calculated to be 1.9×10^{-2} , 1.9×10^{-4} , and 1.2×10^{-6} , respectively, as shown in Fig. 4, using the value of λ obtained from the Raman spectrum ($\lambda_{\text{Raman}} = 2.0 \times 10^{-2}$), which semi-quantitatively agrees with that from TPD analysis ($\lambda_{\text{TPD}} = 4.2 \times 10^{-2}$) as shown in Table 1. λ_{TPD} is proportional to $\lambda_{\text{Raman}}^{1/2}$ (Fig. S5). The values of λ_{TPD} , λ_{Raman} (Table 1), and P_n (Fig. 4) indicate that the density of defects in **NPCs** are two orders of magnitude lower than that in **ZTC**, a nanoporous carbon material with a well-defined structure (see ESI for details).

NPGs obtained by annealing of **NPCs** at a temperature of 1800 °C retain the single-layer graphene structure, as confirmed by the TEM images (Fig. S6) and nanoporosity (Table 1). The measured Raman spectra and deconvoluted peaks of **NPGs** are shown in Figs. 2c and 2d. There also exist eight pronounced peaks in the spectra, including the D band at 1330–1340 cm^{-1} , while the small N_{total} of **NPG** by TPD analysis (0.16–0.39 mmol g^{-1} , Table 1) suggests very few edge defects. The nitrogen sorption isotherms of **NPGs** (Fig. S1) are classified as type IV with a distinct hysteresis loop, and the S_{BET} values derived from the

Table 1 Intensity ratio of the major bands in the Raman spectra and structural parameters of **NPCs**, **NPGs**, and **ZTC** with various templates.

set	I_D/I_D'	I_D/I_G	I_G/I_G	S_{BET}^a $/\text{m}^2 \text{g}^{-1}$	$d_{\text{p,BJH}}^b$ $/\text{nm}$	n_{gra}	N_{total}^a $/\text{mmol g}^{-1}$	λ_{TPD}^b	λ_{Raman}^c
NPC (θ - Al_2O_3)	5.33	2.12	0.43	2.3×10^3 ^[2]	9.2 ^[2]	1.05 ^[2]	3.1 ^[2]	4.2×10^{-2}	2.0×10^{-2}
NPC (γ - Al_2O_3)	5.07	2.31	0.48	2.0×10^3	6.9	1.13 ^d	---	---	1.7×10^{-2}
NPC (stacked) ^e	9.44	1.81	0.30	1.4×10^3	6.2	1.61	---	---	2.4×10^{-2}
NPG (θ - Al_2O_3)	5.12	1.68	1.39	1.9×10^3 ^[2]	9.0 ^[2]	---	0.16 ^[2]	2.6×10^{-3}	1.1×10^{-3}
NPG (γ - Al_2O_3)	5.31	1.67	1.45	2.3×10^3	6.2	---	0.53	7.4×10^{-3}	1.1×10^{-3}
NPG (stacked) ^e	4.12	0.90	1.37	1.0×10^3	6.0	---	---	---	4.9×10^{-4}
ZTC (γ) ^e	---	0.74	0.11	3.6×10^3	~ 1 ^[37]	---	15.4 ^[17]	1.5×10^{-1}	1.1×10^0

^a amount of evolved gases determined by TPD analysis (Fig. S2); ^b defined as the number of defects per hexagon based on S_{BET} , N_{total} , and the area of the graphene's hexagon $S_{\text{h}} = 0.0523 \text{ nm}^2$. λ_{TPD} values estimate the defects at the edges of **NPGs**; ^c derived from the deconvolution of the original Raman spectra shown in Fig. 2; ^d determined by the thermogravimetric analysis of the carbon/alumina composites as shown in Fig. S3; ^e the Raman spectra are shown in Fig. S4.

isotherms were maintained after annealing (Table 1). The XRD patterns of **NPGs** also show a faint and broad 002 peak, while maintaining the 10 diffraction peaks (Fig. 3) These all suggest that **NPGs** also mainly consist of slightly disordered mono-layered graphene.

The amount of vacancies and SW defects in **NPGs** is lower than that of **NPCs**, as confirmed by both Raman and TPD analysis (Table 1). The narrower the linewidth Γ becomes, the lower the defect density will be.⁵³ The Γ_i values of **NPGs** are smaller than those of **NPCs** for all observed bands, as shown in Table S1 and Fig. 2. I_G/I_G increases to more than 1.3 in all **NPGs**, which can be used as an indicator of **NPG** formation.

Annealing reduces the vacancy defects and creates new grain boundaries (Fig. 5), which is consistent with the fact that the position of the D band is almost the same⁵⁸ after thermal treatment (Table S2). For the single-layered **NPGs**, both vacancies and grain boundaries remain: The value of $I_D/I_{D'}=5.33$ (Table 1) is in between the values of vacancy (~ 7) and grain boundary (~ 3.5).⁵¹ For the stacked **NPG** (**NPG** (stacked)), most of the vacancies are removed. The parent stacked **NPC** (**NPC** (stacked)) has $I_D/I_{D'}=9.4$ (Table 1), which indicates that it has both sp^3 ($I_D/I_{D'} \sim 13$)⁴⁶ and vacancy defects (~ 7). The annealing reduced the $I_D/I_{D'}$ value changed to 4.12, which is close to the value of grain boundary (~ 3.5).⁵¹

The mean distance between the defects in **NPGs** (R_{NPG}) can also be estimated using I_D/I_G . The I_D/I_G of 1.7 for θ - and γ -**NPGs** corresponds to $R_{NPG} = 7.0$ nm, from Eq. 2. These values indicate that there exist vacancy and SW defects *per* 9×10^2 hexagonal rings in **NPGs** on average. The λ_{Raman} for θ - and γ -**NPGs** is calculated to be 1.1×10^{-3} , which agrees with λ_{TPD} . The defect density decreases to $\lambda_{TPD}(\text{NPG}) / \lambda_{TPD}(\text{NPC}) \approx \lambda_{Raman}(\text{NPGs}) / \lambda_{Raman}(\text{NPCs}) = 4\text{--}6\%$ upon annealing **NPCs**. The formation of multiple defects on a hexagonal ring is negligible in all **NPGs** as in **NPCs** (Fig. 2). The red shifts of the SW and SW+D bands in **NPGs** may reflect (i) the strain release by defect healing around the last SW sites and/or (ii) the creation of fewer SW defects in the new grain boundary.

The structural analyses of the graphene-based materials using Raman spectroscopy and TPD techniques complement each other. The Raman spectra can be used to investigate the concentration of surface defects such as SW and point defects. The TPD technique is suitable for analyzing the concentration of defects at the edges and adatoms of carbon materials, based on the detection of evolved gases such as H_2 , H_2O , CO , and CO_2 . Further investigation using Raman spectroscopy coupled with the direct observation of defects by high-resolution TEM will be a powerful means of exploring more sophisticated materials.^{59,60}

Conclusions

In this work, we revisited the Raman spectra of **NPCs** and **NPGs** with aids of TPD, XRD, and nitrogen physisorption analysis. Both **NPCs** and **NPGs** mainly consisted of single-layer graphene sheet, whose major surface defects were single vacancies and grain boundaries. SW defects were also observed in all of them. The mean density of vacancy defects *per* hexagon in the graphene framework was 10^{-2} for **NPCs** and $10^{-3}\text{--}10^{-4}$ for **NPGs**, validating their chemical and electrochemical stability. Surface

defect healing will be the basis for controlling and understanding the structure of new **NPG** analogues in future.

Acknowledgement

This work was supported by Grants-in-Aid (19K15281), the Eb-ara-Hatakeyama Memorial Foundation, and Ensemble Grant for Early Career Researchers (Tohoku University). γ - Al_2O_3 nanoparticles were provided by Sasol Chemicals. We thank the helpful and valuable comments of Prof. R. Saito. The authors acknowledge Dr. K. Nomura for technical support on the synthesis of **NPGs**, Dr. R. Tang for physisorption analysis, Dr. H. Nishihara for his advice, and Prof. M. Kakihana for Raman spectroscopy. Generous support from Prof. T. Kyotani and Prof. I. Yamanaka is deeply acknowledged.

Conflicts of interest

The authors declare that they have no conflict of interest.

References

1. M. Yamamoto, Q. Zhao, S. Goto, Y. Gu, T. Toriyama, T. Yamamoto, H. Nishihara, M. Tamura, K. Tomishige, A. Aziz, R. Crespo-Otero, D. Di Tommaso, T. Kyotani and K. Yamazaki, *Chem. Sci.*, 2022, **13**, 3140–3146.
2. M. Yamamoto, S. Goto, R. Tang, K. Nomura, Y. Hayasaka, Y. Yoshioka, M. Ito, M. Morooka, H. Nishihara and T. Kyotani, *ACS Appl. Mater. Interfaces*, 2021, **13**, 38613–38622.
3. Q. Zhao, M. Yamamoto, K. Yamazaki, H. Nishihara, R. Crespo-Otero and D. Di Tommaso, *Phys. Chem. Chem. Phys.*, 2022, **24**, 23357–23366.
4. H. Nishihara, T. Simura, S. Kobayashi, K. Nomura, R. Berenguer, M. Ito, M. Uchimura, H. Iden, K. Arihara, A. Ohma, Y. Hayasaka and T. Kyotani, *Adv. Funct. Mater.*, 2016, **26**, 6418–6427.
5. K. Nomura, H. Nishihara, M. Yamamoto, A. Gabe, M. Ito, M. Uchimura, Y. Nishina, H. Tanaka, M. T. Miyahara and T. Kyotani, *Nat. Commun.*, 2019, **10**, 2559.
6. K. Nomura, H. Nishihara, N. Kobayashi, T. Asada and T. Kyotani, *Energy Environ. Sci.*, 2019, **12**, 1542–1549.
7. R. Wischert, C. Copéret, F. Delbecq and P. Sautet, *Angew. Chem. Int. Ed.*, 2011, **50**, 3202–3205.
8. S. Sunahiro, K. Nomura, S. Goto, K. Kanamaru, R. Tang, M. Yamamoto, T. Yoshii, J. N. Kondo, Q. Zhao, A. G. Nabi, R. Crespo-Otero, D. Di Tommaso, T. Kyotani and H. Nishihara, *J. Mater. Chem. A*, 2021, **9**, 14296–14308.
9. M. Danielis, S. Colussi, C. de Leitenburg, L. Soler, J. Llorca and A. Trovarelli, *Angew. Chem. Int. Ed.*, 2018, **57**, 10212–10216.
10. Y.-C. Lin, C.-C. Lu, C.-H. Yeh, C. Jin, K. Suenaga and P.-W. Chiu, *Nano Lett.*, 2012, **12**, 414–419.
11. K. V. Zakharchenko and A. V. Balatsky, *Carbon*, 2014, **80**, 12–18.
12. C. Hu, S. Sedghi, A. Silvestre-Albero, G. G. Andersson, A. Sharma, P. Pendleton, F. Rodríguez-Reinoso, K. Kaneko and M. J. Biggs, *Carbon*, 2015, **85**, 147–158.
13. Y. Shen, P. Liu, J. Du, Y. Song, H. Cao, M. Zhao, P. Gao, B. Xu, J. Guo and Y. Wu, *Carbon*, 2020, **166**, 388–395.
14. X. Zhang, F. Gärisch, Z. Chen, Y. Hu, Z. Wang, Y. Wang, L. Xie, J. Chen, J. Li, J. V. Barth, A. Narita, E. List-Kratochvil, K. Müllen and C.-A. Palma, *Nat. Commun.*, 2022, **13**, 442.
15. C. Senger, X. Fan, J. N. Pagaduan, X. Zhang, J. Ping and R. Katsumata, *Small*, 2023, **19**, 2206295.

16. K. Pirabul, Z.-Z. Pan, R. Tang, S. Sunahiro, H. Liu, K. Kanamaru, T. Yoshii and H. Nishihara, *Bull. Chem. Soc. Jpn.*, 2023, **96**, 510-518.
17. R. Tang, M. Yamamoto, K. Nomura, E. Morallón, D. Cazorla-Amorós, H. Nishihara and T. Kyotani, *J. Power Sources*, 2020, **457**, 228042.
18. Z. Shen, W. Yu, A. Aziz, K. Chida, T. Yoshii and H. Nishihara, *J. Phys. Chem. C*, 2023, **127**, 6239–6247.
19. T. Xia, T. Yoshii, K. Nomura, K. Wakabayashi, Z.-Z. Pan, T. Ishii, H. Tanaka, T. Mashio, J. Miyawaki, T. Otomo, K. Ikeda, Y. Sato, M. Terauchi, T. Kyotani and H. Nishihara, *Chem. Sci.*, 2023, **14**, 8448–8457
20. J. Campos-Delgado, Y. A. Kim, T. Hayashi, A. Morelos-Gómez, M. Hofmann, H. Muramatsu, M. Endo, H. Terrones, R. D. Shull, M. S. Dresselhaus and M. Terrones, *Chem. Phys. Lett.*, 2009, **469**, 177-182.
21. M. S. Dresselhaus, A. Jorio, A. G. Souza Filho and R. Saito, *Philosophical Transactions of the Royal Society A: Mathematical, Physical and Engineering Sciences*, 2010, **368**, 5355-5377.
22. L. G. Cançado, A. Jorio, E. H. M. Ferreira, F. Stavale, C. A. Achete, R. B. Capaz, M. V. O. Moutinho, A. Lombardo, T. S. Kulmala and A. C. Ferrari, *Nano Lett.*, 2011, **11**, 3190-3196.
23. X. Jia, J. Campos-Delgado, M. Terrones, V. Meunier and M. S. Dresselhaus, *Nanoscale*, 2011, **3**, 86-95.
24. P. Solís-Fernández and H. Ago, *ACS Appl. Nano Mater.*, 2022, **5**, 1356-1366.
25. A. M. Rao, E. Richter, S. Bandow, B. Chase, P. C. Eklund, K. A. Williams, S. Fang, K. R. Subbaswamy, M. Menon, A. Thess, R. E. Smalley, G. Dresselhaus and M. S. Dresselhaus, *Science*, 1997, **275**, 187-191.
26. R. Saito, A. Jorio, A. G. Souza Filho, G. Dresselhaus, M. S. Dresselhaus and M. A. Pimenta, *Phys. Rev. Lett.*, 2001, **88**, 027401.
27. M. M. Lucchese, F. Stavale, E. H. M. Ferreira, C. Vilani, M. V. O. Moutinho, R. B. Capaz, C. A. Achete and A. Jorio, *Carbon*, 2010, **48**, 1592-1597.
28. I. Childres, L. A. Jauregui, W. Park, H. Cao and Y. P. Chen, *New Developments in Photon and Materials Research, Chapter 19*, Nova Science Publishers, New York, 2013.
29. D. B. Schüpfer, F. Badaczewski, J. Peilstöcker, J. M. Guerra-Castro, H. Shim, S. Firoozabadi, A. Beyer, K. Volz, V. Presser, C. Heiliger, B. Smarsly and P. J. Klar, *Carbon*, 2021, **172**, 214-227.
30. A. V. Gubarevich, R. Tamura and K. Yoshida, *Ceram. Int.*, 2023, **49**, 23887-23892.
31. M. Thommes, K. Kaneko, A. V. Neimark, J. P. Olivier, F. Rodriguez-Reinoso, J. Rouquerol and K. S. W. Sing, *Pure Appl. Chem.*, 2015, **87**, 1051-1069.
32. K. Kaneko, C. Ishii, M. Ruike and H. Kuwabara, *Carbon*, 1992, **30**, 1075-1088.
33. A. Gupta, G. Chen, P. Joshi, S. Tadigadapa and P. C. Eklund, *Nano Lett.*, 2006, **6**, 2667-2673.
34. A. Das, S. Pisana, B. Chakraborty, S. Piscanec, S. K. Saha, U. V. Waghmare, K. S. Novoselov, H. R. Krishnamurthy, A. K. Geim, A. C. Ferrari and A. K. Sood, *Nat. Nanotech.*, 2008, **3**, 210-215.
35. S. Berciaud, S. Ryu, L. E. Brus and T. F. Heinz, *Nano Lett.*, 2009, **9**, 346-352.
36. M. Rahaman, R. D. Rodriguez, G. Plechinger, S. Moras, C. Schüller, T. Korn and D. R. T. Zahn, *Nano Lett.*, 2017, **17**, 6027-6033.
37. Z. Ma, T. Kyotani and A. Tomita, *Chem. Commun.*, 2000, 2365-2366.
38. F. Banhart, J. Kotakoski and A. V. Krashennnikov, *ACS Nano*, 2011, **5**, 26-41.
39. A. Hashimoto, K. Suenaga, A. Gloter, K. Urita and S. Iijima, *Nature*, 2004, **430**, 870-873.
40. J. Guo, J. R. Morris, Y. Ihm, C. I. Contescu, N. C. Gallego, G. Duscher, S. J. Pennycook and M. F. Chisholm, *Small*, 2012, **8**, 3283-3288.
41. K. Suenaga, H. Wakabayashi, M. Koshino, Y. Sato, K. Urita and S. Iijima, *Nat. Nanotech.*, 2007, **2**, 358-360.
42. T. Fujimori, K. Urita, T. Ohba, H. Kanoh and K. Kaneko, *J. Am. Chem. Soc.*, 2010, **132**, 6764-6767.
43. K. Yamazaki, N. Niitsu, K. Nakamura, M. Kanno and H. Kono, *J. Phys. Chem. A*, 2012, **116**, 11441-11450.
44. S. K. Tiwari, S. K. Pandey, R. Pandey, N. Wang, M. Bystrzejewski, Y. K. Mishra and Y. Zhu, *Small*, 2023, **n/a**, 2303340.
45. M. Toyoda, S. Hou, Z.-H. Huang and M. Inagaki, *Carbon Lett.*, 2023, **33**, 335-362.
46. A. C. Ferrari, J. C. Meyer, V. Scardaci, C. Casiraghi, M. Lazzeri, F. Mauri, S. Piscanec, D. Jiang, K. S. Novoselov, S. Roth and A. K. Geim, *Phys. Rev. Lett.*, 2006, **97**, 187401.
47. T. X. Nguyen and S. K. Bhatia, *Langmuir*, 2004, **20**, 3532-3535.
48. F. Ming and A. Zangwill, *Phys. Rev. B*, 2011, **84**, 115459.
49. A. Karlsson, H. Grennberg and S. Johansson, *RSC Adv.*, 2023, **13**, 781-789.
50. C. Thomsen and S. Reich, *Phys. Rev. Lett.*, 2000, **85**, 5214-5217.
51. A. Eckmann, A. Felten, A. Mishchenko, L. Britnell, R. Krupke, K. S. Novoselov and C. Casiraghi, *Nano Lett.*, 2012, **12**, 3925-3930.
52. A. Eckmann, A. Felten, I. Verzhbitskiy, R. Davey and C. Casiraghi, *Phys. Rev. B*, 2013, **88**, 035426.
53. I. Childres, L. A. Jauregui, J. Tian and Y. P. Chen, *New J. Phys.*, 2011, **13**, 025008.
54. T. Fujimori, L. R. Radovic, A. B. Silva-Tapia, M. Endo and K. Kaneko, *Carbon*, 2012, **50**, 3274-3279.
55. T. J. Booth, F. Pizzocchero, H. Andersen, T. W. Hansen, J. B. Wagner, J. R. Jinschek, R. E. Dunin-Borkowski, O. Hansen and P. Bøggild, *Nano Lett.*, 2011, **11**, 2689-2692.
56. M. S. H. Boutilier, C. Sun, S. C. O'Hern, H. Au, N. G. Hadjiconstantinou and R. Karnik, *ACS Nano*, 2014, **8**, 841-849.
57. H. Kraus, D. Simin, C. Kasper, Y. Suda, S. Kawabata, W. Kada, T. Honda, Y. Hijikata, T. Ohshima, V. Dyakonov and G. V. Astakhov, *Nano Lett.*, 2017, **17**, 2865-2870.
58. K.-D. Park, M. B. Raschke, J. M. Atkin, Y. H. Lee and M. S. Jeong, *Adv. Mater.*, 2017, **29**, 1603601.
59. A. L. Mackay and H. Terrones, *Nature*, 1991, **352**, 762-762.
60. Y. Ito, Y. Tanabe, H. J. Qiu, K. Sugawara, S. Heguri, N. H. Tu, K. K. Huynh, T. Fujita, T. Takahashi, K. Tanigaki and M. Chen, *Angew. Chem. Int. Ed.*, 2014, **53**, 4822-4826.